ELSEVIER

Composites Science and Technology 62 (2002) 1105–1112

COMPOSITES SCIENCE AND TECHNOLOGY

www.elsevier.com/locate/compscitech

Distribution and alignment of carbon nanotubes and nanofibrils in a polymer matrix

Carole A. Cooper[a,*], Diana Ravich[a], David Lips[b], Joerg Mayer[b], H. Daniel Wagner[a]

[a] *Weizmann Institute of Science, Department of Materials and Interfaces, Rehovot 76100, Israel*
[b] *ETH Zürich, Biokompatible Werkstoffe und Bauweisen, Wagistrasse 23, CH-8952 Schlieren, Switzerland*

Received 20 September 2001; received in revised form 27 February 2002; accepted 13 March 2002

Abstract

Composites consisting of different quantities of carbon nanotubes and nanofibrils in a poly(methyl methacrylate) (PMMA) matrix have been prepared using a polymer extrusion technique. The nanotubes or nanofibrils were first dispersed over the polymer matrix particles using a dry powder mixing method. The final composite specimens contained well-dispersed and aligned nanofibrils and nanotubes. The orientation distribution of carbon fibrils and nanotubes in the composite was determined by image analysis and found to be maximized in the extrusion flow direction. The Knoop hardness data confirmed this observation, as a maximum was observed at 90° to the orientation of the reinforcement. When the initial PMMA particle diameter was under 200 μm, considerable improvements were observed in the mechanical properties of the nanofibril/PMMA composites. The interpretation of the mechanical data for nanotube/PMMA composites was more complex. Indeed, the tensile modulus was almost insensitive to the presence of either single-wall or multi-wall nanotubes, whereas the impact strength (thus, indirectly, the fracture toughness) was significantly improved by even small amounts of single-wall nanotubes. The method proposed here for the dispersion and orientation of carbon nanotubes and nanofibrils in a polymer matrix show promise for the preparation of improved engineering composites.

Keywords: Carbon nanofibrils; B. Mechanical properties

1. Introduction

Carbon nanotubes have attracted considerable scientific attention because of their unique physical properties [1–6]. They have diameters in the nanometer scale, are up to tens of microns long, and can be single- or multi-walled (SWNT and MWNT, respectively). Compared with carbon fibers, which typically have a Young's modulus of up to 750 GPa, the elastic modulus of carbon nanotubes has been measured to be approximately 1–2 TPa [1,4]. The strength of carbon nanotubes has been reported to be about two order of magnitude higher than current high-strength carbon fibers [4,6]. Carbon nanofibrils are sized somewhere in-between carbon fibers and nanotubes (150–200 nm diameter, hundreds of microns long) and their mechanical properties have not been extensively studied but are thought to be limited by a relatively large amount of microstructural defects. Thus carbon nanotubes, and possibly nanofibrils, may offer an attractive alternative to carbon fibers because of their small diameter, large aspect ratio, and intrinsically high mechanical properties (provided, however, that an effective interface is able to provide stress transfer to the reinforcing carbon phase, an aspect that remains to be studied altogether). Composites using such nanoscale reinforcements could potentially be processed into intricately shaped components using traditional methods such as injection molding and extrusion, which in general is more difficult or impossible with the larger, micron-scale carbon fibers. On the other hand, the known problem of nanofibrils/nanotubes dispersion must be solved to achieve this objective. Producing well-dispersed carbon nanofibrils/nanotubes in a composite is difficult because the addition of a small amount of solid 'powder' (carbon) in a comparatively large amount of liquid polymer in the early mixing stages often leads to phase separation between the carbon and polymer matrix: the nanotubes/

* Corresponding author. Tel.: +972-8-934-2244; fax: +972-8-934-4137.
E-mail address: carole_a_cooper@hotmail.com (C.A. Cooper).

0266-3538/02/$ - see front matter
PII: S0266-3538(02)00056-8

nanofibrils are more attracted to each other (for example, due to van der Waals forces between SWNTs) than to the liquid. The time scale necessary for matrix polymerization (i.e. to 'lock' the carbon particles into a dispersed final position) may be too large and phase separation or clustering occurs. In the present work we propose to prepare the nanocomposites by means of a dry processing method. The promising mechanical properties of the resulting specimens, prepared by extrusion, demonstrate the potential of the proposed approach.

2. Materials and methods

2.1. Basic components

The matrix used was poly (methyl methacrylate), (PMMA, Plexiglas G8E, supplied by Victrex, Germany) obtained as dry spherical particles 100–500 μm in diameter. The carbon nanofibrils (Pyrograf-III carbon nanofiber, supplied by Applied Sciences Inc., Ohio, USA) were pyrolitically stripped and therefore had no surface organic contamination. The diameter of fibril was 200 nm, and the length range was 200–500 μm. The MWNT (diameter range: 10–15 nm; length range: 2–3 μm) were obtained from Dynamic Enterprises Ltd, UK, and the SWNT (diameter range: 1.4–2 nm; length range: 200–400 μm) were purchased from Tubes@Rice, Texas, USA.

2.2. Composite preparation

The components were mixed using a high intensity ultrasonic processor (Vibracell VCX 600), first separately (thus, the nanotubes or nanofibrils with a small amount of ethanol, and the PMMA with a small amount of ethanol) at 10% amplitude for 90 s, then together first mechanically then by sonication at 50% amplitude for 90 s. This promoted the distribution of carbon fibrils/nanotubes over the surface of the PMMA spherical particles, and prevented particle clustering. After sonication the mix was spread out thinly on a foil surface and dried in a vacuum oven at 50 °C for 1–2 h to remove any trace of ethanol, then mechanically mixed using a Molinex Attritor (Netzsch Feinmahl-Technik, Germany) that consisted of a high torque electric engine, a three-blade propeller and a receptacle half-filled with stainless steel spheres of a diameter of 5 mm. The material to be mixed was located in the gaps between the steel spheres. The attritor propeller had three de-phased blades, and was operated at 2000 rpm for 30 min. A Jeol JSEM 6400 operating at 12 kV was used to obtain images of the polymer particles (with and without nanofibrils). The same electron microscope was also used at a later stage to observe the fracture surface of a broken specimen following mechanical testing. An Edwards 5150 sputtering system operating at 10 mA (12 min) was used to coat the specimens with gold to avoid charging on the specimen and beam damage. Fig. 1 shows the PMMA particles before and after mixing. The mixing was followed by kneading at a temperature of 170 °C with a Brabender Plasti-Corder (a laboratory-sized twin-screw compounder, speed range of 30–50 rpm for 10–30 min). As a result of kneading, the matrix spherical particles fused together to become a uniform viscous mass. These conditions allowed high shear stresses to act on the polymer to further improve the distribution of the reinforcement within the matrix and also separated out any remaining clusters of nanofibrils

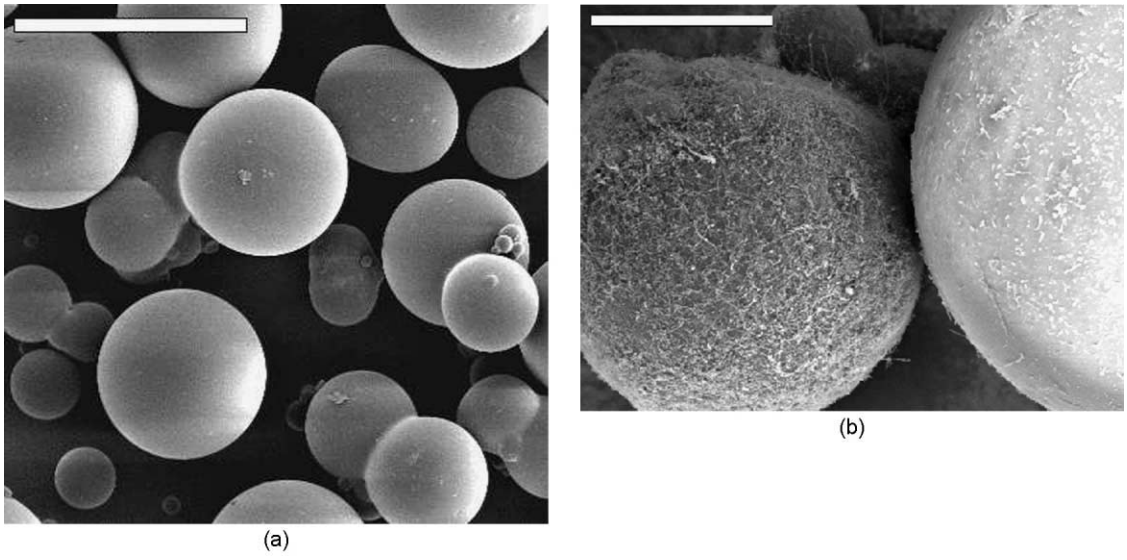

Fig. 1. (a) SEM micrograph of as-received PMMA particles (scale bar: 200 μm); (b) SEM micrograph of PMMA particles with nanofibrils spread over the surface (4 wt.% nanofibrils, PMMA particles under 200 μm diameter) (scale bar: 50 μm).

and nanotubes. The reference sample of pure PMMA was not sonicated with ethanol or mixed in the Brabender kneader prior to extrusion. These steps were only taken to incorporate the carbon particles into the matrix. We made no distinction between particle sizes for the pure PMMA because here, particle surface area was not important (as it is when mixing with the carbon particles) as it would be in effect, pure matrix.

Following kneading, the final step of composite preparation was to extrude the "pre-mixes" in a small laboratory extruder to orient the reinforcement in the flow direction. The apparatus was a Brabender DSK 25 single-screw extruder with 25 mm screw diameter and a L/D ratio of 22. The melt temperature was 232 °C, and the pressure was 16 bar in the first stage. The composite was drawn off from the extruder slit die and quickly quenched with water. The efficiency of the preparation method for orienting the reinforcement was determined using two methods:

(i) Image analysis (NIH Image [7]): the effectiveness of image analysis for the measurement of fiber orientation distribution in short-fiber composites has been demonstrated elsewhere [8,9]. The final composite specimens were microtomed into thin (70–100 nm) films at 90° to the extrusion flow direction, using a diamond knife (Micro Star Co.) and a Reichert-Jung Ultracut microtome (at room temperature). Slicing the specimens at 90° to the flow direction ensured that the cutting blade did not induce any changes in reinforcement orientation. The slices were placed on copper grids and examined by TEM using a Philips CM120 at 120 kV. The TEM micrographs were then used to measure the angular distribution of the nanofibrils or nanotubes with respect to the microtome direction. Regarding the nanotube orientation, only MWNT-containing specimens were examined, as the weight content of SWNT-containing specimens was too small.

(ii) Knoop hardness test: this test, which is sensitive to material anisotropy because of the elongated shape of the indenter tip, has been used previously to assess the anisotropic microhardness and Young's modulus of small-scale polymeric areas [10–12]. It was used here only to assess the degree of fibril/tube orientation. The specimen surfaces (top surface parallel to the extrusion direction) were carefully polished until a smooth surface was obtained. Polishing was performed using a Buehler Minimet apparatus, using 320, 400 and 620 grit abrasive paper, followed by 6 and 1 μm diamond paste and finally with 0.05 μm alumina paste. Microindentations were performed using a Leitz microhardness tester attached to an optical microscope (Leitz Metallux 3) equipped with a video imaging system. Indentations were produced using a Knoop indenter with an applied load of 0.5 N and using a 10 s loading cycle, both parallel (0°) and perpendicular (90°) to the direction of extrusion. The lengths of the imprinted diagonals were measured within 30 s after indentation using a Leitz hardness-measuring digital eyepiece equipped with a Leitz computer counter printer (RZO-DO). The Knoop microhardness (H_k) values were calculated according to the formula:

$$H_k = 14.23\frac{P}{d^2}10^{-6}$$

where H_k = Knoop microhardness (MPa), P = applied force (N), d = long diagonal measurement (m).

Fifteen imprints were made at 0° and 90° to the extrusion direction for each type of composite.

2.3. Static and dynamic tensile testing

The tensile properties of the composites were investigated using static and dynamic tensile testing. These tests were performed on 30 mm×4 mm×0.3 mm extruded strips using a gauge length of 20 mm, with the tensile load directed parallel to the extrusion direction. For the static tensile tests, the tensile test speed was 130 μm per minute on a home made mini-tensile testing machine. The tensile impact tests were performed with a Zwick pendulum apparatus (0.5 J) using double-notched specimens (notch depth: 0.4 mm).

3. Results and discussion

The role of initial particle size of PMMA matrix was looked into, especially its effect on the reinforcement distribution and mechanical properties of the composite. The more traditional effects of amount and type of reinforcement were also studied. The 'as received' PMMA powder was divided into two fractions by sieving through a 200 μm sized mesh. Fig. 1(a) shows a SEM micrograph of the smaller size fraction of PMMA particles (thus, under 200 μm). Note the variation in particle size. Fig. 1(b) shows the homogeneous distribution of nanofibrils over the PMMA particles, following the ultrasonication step described in the experimental section. The 10 wt.% nanofibril composite was prepared with PMMA particles below 200 μm only. This is because we had limited amount of those particular nanofibrils. We chose the particles below 200 μm as the SEM micrographs showed that there was good coverage of the carbon particles over the PMMA surface.

Transmission electron microscopy (TEM) was used to determine the distribution and alignment of the nanofibrils, and particularly nanotubes, in the PMMA matrix of the final composites. Two examples of the TEM micrographs can be seen in Fig. 2(a) for the 10 wt.% nanofibrils in PMMA and Fig. 2(b) for the 4 wt.% MWNTs in PMMA. Both the nanofibrils and nanotubes

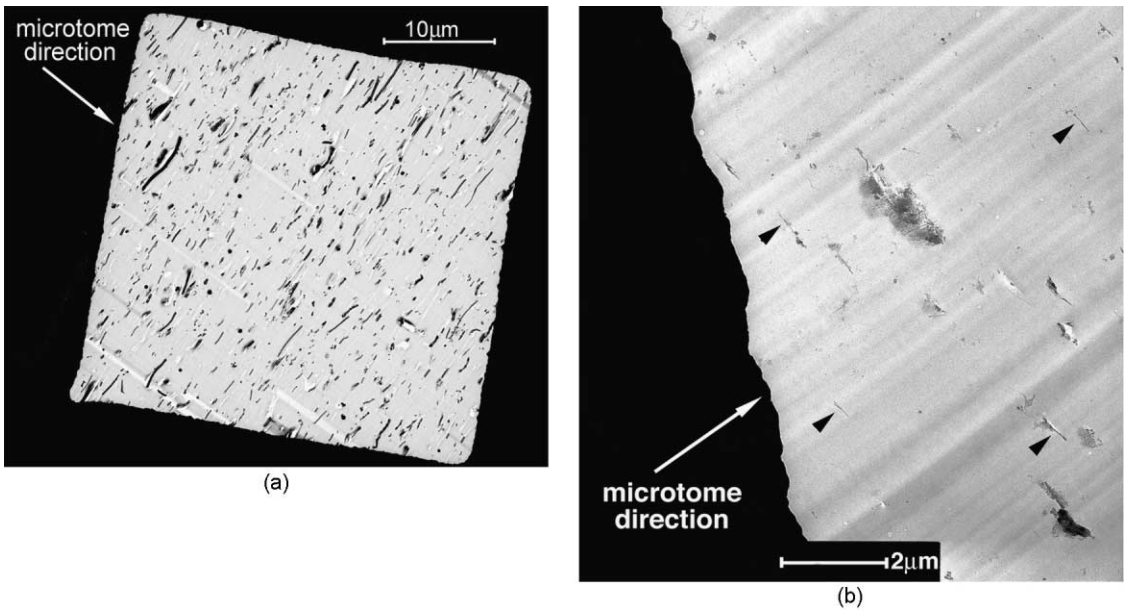

Fig. 2. (a) TEM micrograph of 10 wt.% nanofibrils in PMMA; (b) 4 wt.% MWNTs in a PMMA matrix (the small arrows indicate the MWNTs). Specimens were microtomed at 90° to the extrusion direction, and the large arrows on both micrographs indicate the microtome cutting direction.

were found to be well distributed within the matrix and to have good alignment. The composites were microtomed at approximately 90° to the extrusion direction, and the orientation distribution was measured with respect to the microtoming cutting marks, refer to Fig. 2(a) and (b). The resulting histograms for 0.1, 4 and 10 wt.% nanofibrils and 4 wt.% MWNTs can be seen in Fig. 3(a)–(d) respectively. The mean, standard deviation and full width at half maximum (FWHM) of the data for each plot (taken from a Lorentzian fit of the data) are presented in Table 1. Overall, the orientation distribution of carbon fibrils and nanotubes in the composite as determined by image analysis is found to be maximized in the extrusion flow direction. As seen from Fig. 3(a)–(c), there is more spread in the orientation distribution with increased nanofibril content (from 0.1 to 10 wt.%). A possible cause for this may be that the addition of nanofibrils increases the likelihood that these can tangle and interfere with each other in the melt. It may also be that there was more incidence of clusters in the 10 wt.% nanofibrils that had not broken down during the sonication and kneading processes. In the case of MWNTs [Fig. 3(d)], the distribution, although not as narrow as the 0.1 wt.% nanofibrils, is still less than that of the 4 wt.% nanofibrils. In this case, the nanotubes had a much larger aspect ratio than the nanofibrils, which might have increased the influence of the matrix (through its increased contact surface area) on the nanotubes. The orientation distribution of SWNTs in PMMA was not considered by TEM due to their very low concentration, as the measurement error was considered to be too large.

The Knoop hardness data confirm the conclusions reached by TEM observations and image analysis. Indeed, a maximum is observed at 90° to the orientation of the reinforcement. The geometrical details of the Knoop indenter and indentation direction with respect to the orientation of the reinforcement are shown in Fig. 4. The results of the Knoop hardness testing on the nanofibril and nanotube composites are presented in Fig. 5(a) and (b), respectively. For all specimens, the Knoop hardness is at a maximum when the long diagonal is perpendicular to the reinforcement orientation. Thus the orientation of the reinforcement can be detected by hardness measurements that are sensitive to the anisotropy of the material.

The Young's moduli of nanofibril- and nanotube-based composites are presented in Fig. 6(a) and (b).

Table 1
Statistical data for the histograms in Fig. 3, using a Lorentzian fit to the data

Specimen	Mean (°)	Standard deviation (°)	Full width at half maximum (°)
PMMA + 0.1 wt.% nanofibrils	95	7	6
PMMA + 4 wt.% nanofibrils	87	14	16
PMMA + 10 wt.% nanofibrils	83	30	35
PMMA + 4 wt.% MWNT	90	9	12

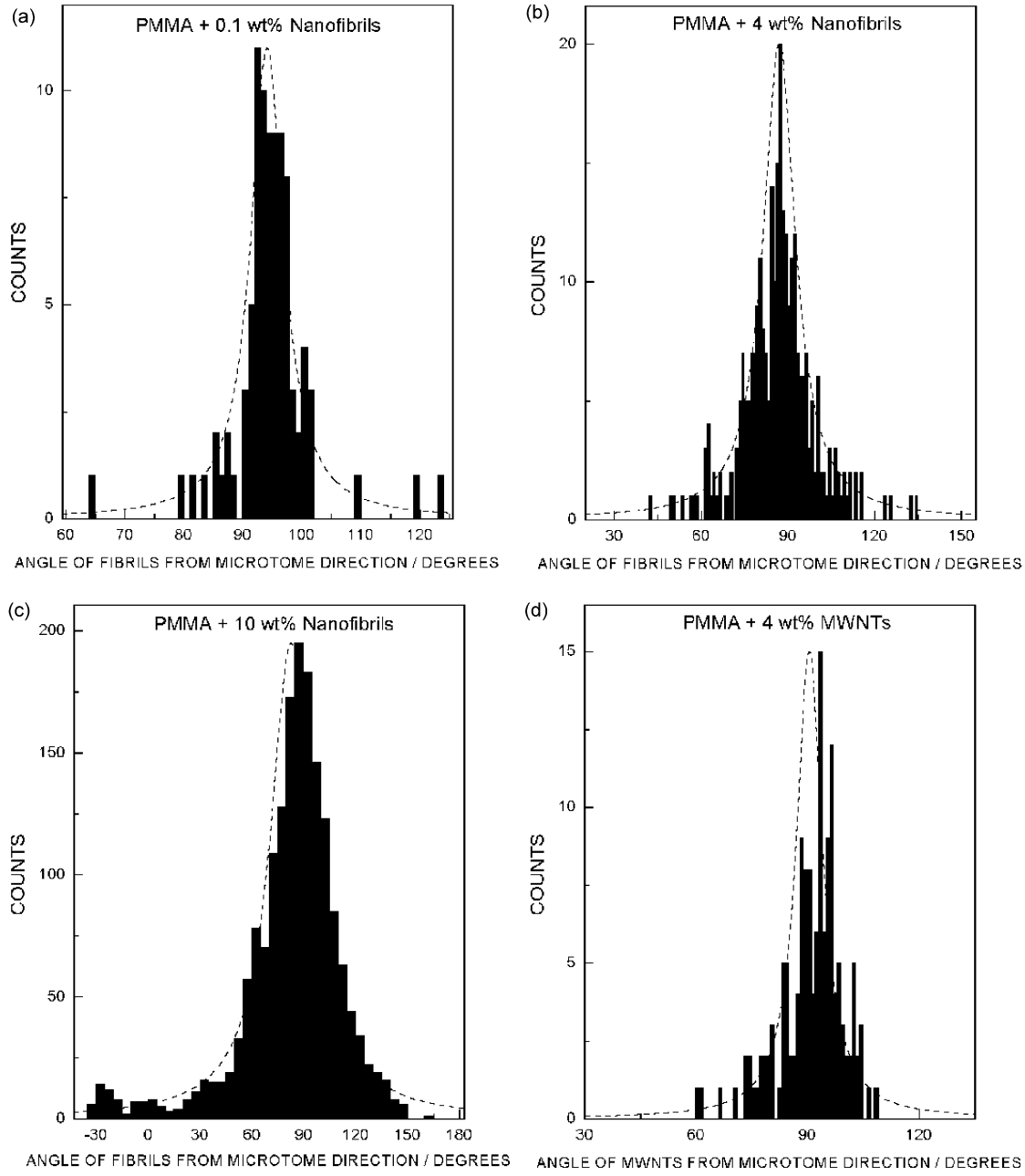

Fig. 3. Orientation distribution histograms: (a) PMMA + 0.1 wt.% nanofibrils, (b) PMMA + 4 wt.% nanofibrils, (c) PMMA + 10 wt.% nanofibrils and (d) PMMA + 4 wt.% MWNTs. A dashed line corresponds to the Lorentzian fit to the data.

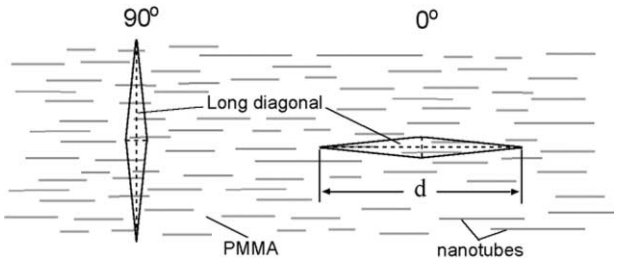

Fig. 4. Schematic diagram of the Knoop indentation direction with respect to the orientation of the reinforcement; 'd' denotes the length of the long diagonal.

From Fig. 6(a), the nanofibril composites prepared using PMMA particles with a diameter under 200 μm resulted in a tensile modulus that was higher than that of the unfilled PMMA, at both nanofibril contents of 4 and 10 wt.%, and in spite of the lack of interfacial wetting and/or adhesion. Indeed, Fig. 7 shows a SEM micrograph of the broken surface of a PMMA + 10 wt.% nanofibril specimen following tensile testing. Holes where the nanofibrils have been pulled out of the matrix, and gaps around the base of most nanofibrils, are observed and indicate poor wetting and/or adhesion between the nanofibril and the matrix.

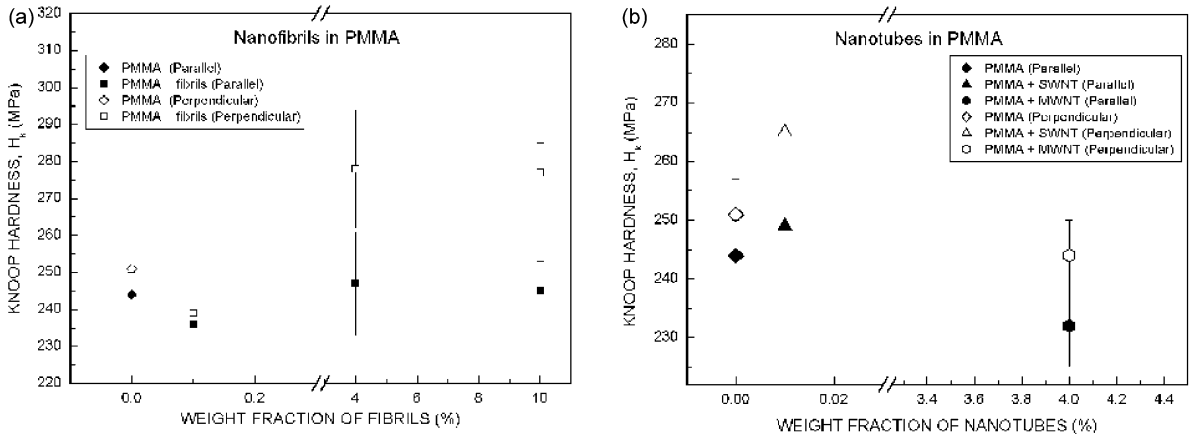

Fig. 5. Variation of Knoop microhardness of (a) nanofibril/PMMA composites and (b) nanotube/PMMA composites, as a function of filler content at 0° (filled symbols), and 90° (open symbols) relative to the reinforcement orientation. All PMMA particles were under 200 μm diameter.

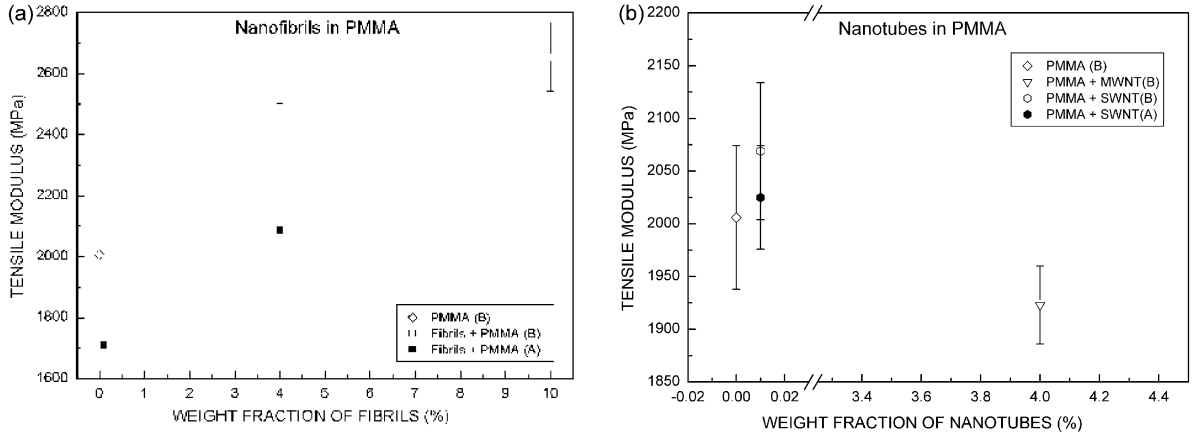

Fig. 6. Variation of Young's modulus for (a) nanofibril/PMMA composites and (b) nanotube/PMMA composites as a function of filler content. (A) designates PMMA particle diameter above 200 μm, (B) designates PMMA particle diameter below 200 μm.

However, from Fig. 6(b), no improvement is observed for the Young's modulus of either types of nanotube-based composites. Based on the modulus improvement for nanofibril composites despite the observed poor wetting/adhesion, as described above, the lack of inherent chemical interaction between MWNT and PMMA, or the possibility that inner SWNTs are sliding past each other preventing effective load transfer [13,14], may hardly be invoked to explain this result. Finally, a comparison of moduli between composites prepared with PMMA particles larger and smaller than 200 μm shows that the latter leads to composites that perform slightly better. One reason for this might be the increase in surface area of the particles, which allows a better distribution of the nanotubes and nanofibrils over the PMMA surface.

Comparisons were made between the available surface area of PMMA particles (above and below 200 μm diameter) and the surface area of the carbon materials, using the 4 wt.% reinforcement as an example. The total surface area of PMMA particles is easily calculated as 2.5 m^2 for the theoretical case of particles with a diameter of 100 μm; likewise, it is 0.7 m^2 for the theoretical case of particles with a diameter of 350 μm. For 4 wt.% nanofibrils, the total surface area is 11 m^2 and for 4 wt.% MWNTs it is 239 m^2. Clearly, once the PMMA

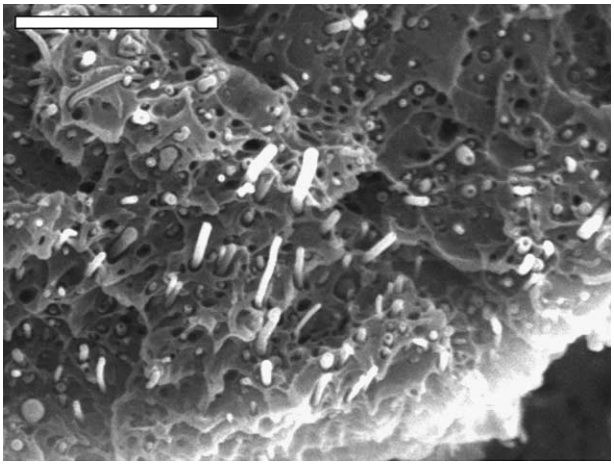

Fig. 7. SEM micrograph of the fracture surface of a PMMA + 10 wt.% nanofibril strip following tensile testing (scale bar: 5 μm).

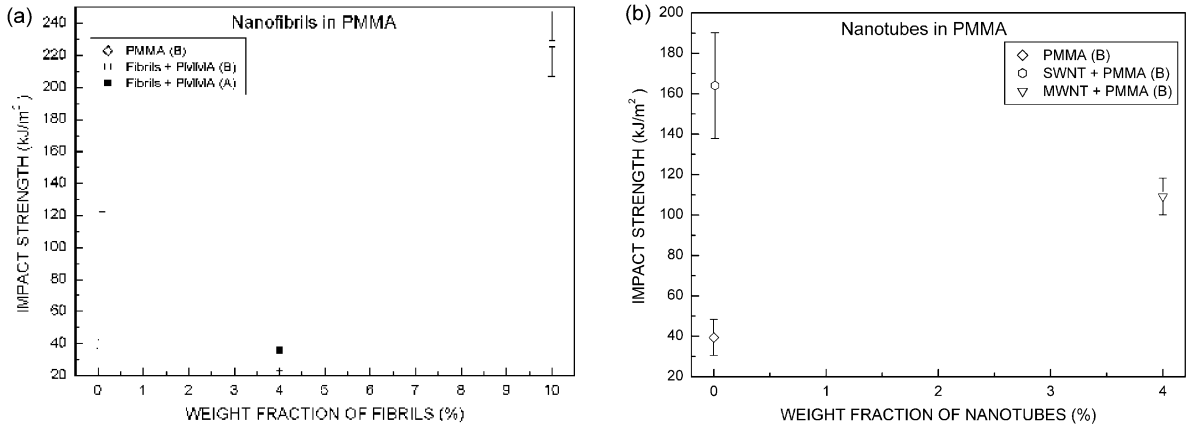

Fig. 8. Impact strength of (a) nanofibril/PMMA composites and (b) nanotube/PMMA composites, as a function of filler content. (A) designates PMMA particle diameter above 200 μm, (B) designates PMMA particle diameter below 200 μm.

particles are fully covered, there still must be an excess of carbon material in both cases. The excess carbon would tend to cluster together. Such clusters, however, could be dispersed in the attrition/kneading/extrusion process. Optimum dispersion cannot be reached unless all of the carbon material fully adheres to the PMMA particles. For this to happen, either the amount of PMMA would have to be increased (for a fixed amount of carbon) to 0.2 kg for 100 μm PMMA particles and 0.8 kg for 350 μm PMMA particles but this would dramatically decrease the weight% of carbon material. Or, we could keep the amount of both carbon types (4 wt.%) and PMMA (50 g) constant, and calculate the size of PMMA particles we would need to equal the surface area of reinforcement. For nanofibrils (with surface area of 11 m^2), the PMMA particle diameter would have to be 11 μm. For MWNTs (with surface area of 239 m^2), the PMMA particle diameter would have to be 0.5 μm.

The tensile impact data are presented in Fig. 8. From Fig. 8(a), the tensile impact resistance improved for those nanofibril/PMMA composites prepared with under 200 μm PMMA particles. Increasing the fraction of carbon nanofibrils in general also improves the impact properties, at least up to 10 wt.%. Regarding nanotube-based composites, the data presented in Fig. 8(b) shows that the impact resistance of PMMA has been improved considerably (from 40 to 160 kJ/m^2) by the inclusion of just 0.1 wt.% of SWNT (data were obtained only for composites prepared with under 200 μm PMMA particles). The impact resistance of MWNT-based PMMA composites also increased (from 40 to 110 kJ/m^2), with 4 wt.% nanotubes. Impact is loosely related to fracture toughness and, in fiber-based composites, the toughness is inversely proportional to the interfacial adhesion. In other words, the weaker the interfacial adhesion, the higher the toughness. This argument may be invoked here to explain the impact resistance (or toughness) of nanofibril- and nanotube-based composites, based on the apparent lack of interfacial adhesion described earlier in Fig. 7. Moreover, the fracture strain of carbon nanotubes is estimated to be 10–30% [15], allowing extensive bending and buckling [2,4,16]. This high flexibility most probably provides an additional source of higher fracture toughness to the composite. In SWNTs, the pullout and sliding of individual nanotubes within each bundle also adds to the energy absorbing effect. Little research has been performed on the mechanical properties of carbon nanofibril polymer composites but it has been mentioned that individual nanofibrils are also capable of high conformations [17].

4. Conclusions

Carbon nanotube and carbon nanofibril composites have been successfully prepared using a dry powder mixing method followed by a polymer extrusion technique designed to distribute and orient the carbon reinforcement. SEM, TEM and Knoop testing demonstrated the efficiency of this method for distributing and orientating the nanotubes and nanofibrils. When the initial PMMA particle diameter was under 200 μm, considerable improvements were observed in the mechanical properties of the nanofibril/PMMA composites. Interpreting the mechanical data for nanotube/PMMA composites proved more delicate, as the tensile modulus was almost insensitive to the presence of either single-wall or multi-wall nanotubes, whereas the impact strength (thus, indirectly, the fracture toughness) was significantly improved by even small amounts of single-wall nanotubes.

Acknowledgements

This project was supported by the (CNT) Thematic European network on "Carbon Nanotubes for Future

Industrial Composites" (EU), the MINERVA Foundation, the Israel Science Foundation and by the Swiss Federal Institute of Technology. H.D. Wagner is the recipient of the Livio Norzi Professorial Chair. The provision of the nanofibrils (Pyrograf-III carbon nanofiber) from Applied Sciences Inc., OH, USA is gratefully acknowledged.

References

[1] Treacy MMJ, Ebbesen TW, Gibson JM. Exceptionally high Young's modulus observed for individual carbon nanotubes. Nature 1996;381:678–80.
[2] Falvo MR, Clary CJ, Taylor RM, Chi V, Brooks FP, Washburn S, et al. Bending and buckling of carbon nanotubes under large strain. Nature 1997;389:582–4.
[3] Bernholc J, Brabec C, Buongiorno M, Nardelli M, Maiti A, Roland C, et al. Theory of growth and mechanical properties of nanotubes. Appl Phys A 1996;67:39–46.
[4] Lourie O, Cox DM, Wagner HD. Buckling and collapse of embedded carbon nanotubes. Phys Rev Lett 1998;81(8):1638–41.
[5] Zhao Q, Frogley MD, Wagner HD. Using carbon nanotubes to sense matrix stresses around a single glass fiber. Comp Sci Technol 2001;61:2139–43.
[6] Yu M-F, Lourie O, Dyer MJ, Moloni K, Kelly TF, Ruoff RS. Strength and breaking mechanism of multiwalled carbon nanotubes under tensile load. Science 2000;287:637–40.
[7] Public domain program developed at the US National Institutes of Health. Available from the internet by anonymous FTP from zippy.nimh.gov or on floppy disk from the national Technical Information Service, Springfield, VA, part number PB95–500195GEI.
[8] Fischer G, Eyefer P. Measuring spatial orientation of short fiber reinforced thermoplastics by image analysis. Polym Comp 1998; 9(4):297–302.
[9] Jung SW, Kim SY, Nam HW, Han KS. Measurements of fiber orientation and elastic-modulus analysis in short-fiber-reinforced composites. Comp Sci Technol 2001;61:107–16.
[10] Amitay-Sadoskvy E, Wagner HD. Hardness and Young's modulus of transcrystalline polypropylene by Vickers and Knoop microindentation. J Polym Sci: Part B: Polym Phys 1999;37:523–30.
[11] Amitay-Sadoskvy E, Zheng S, Smith J, Wagner HD. Directional indentation of transcrystalline polypropylene. Acta Polymerica 1998;49:588–93.
[12] Perry AJ, Rowcliffe DJ. The microhardness of composite materials. J Mater Sci 1973;9:904–7.
[13] Schadler LS, Giannaris SC, Ajayan PM. Load transfer in carbon nanotube epoxy composites. Appl Phys Lett 1998;73(26):3842–4.
[14] Ajayan PM, Schadler LS, Giannaris C, Rubio A. Single-walled carbon nanotube-polymer composites: strength and weakness. Adv Mater 2000;12(10):750–3.
[15] Yakobson BI, Smalley RE. Fullerene nanotubes: $C_{1,000,000}$ and beyond. Am Sci 1997;85:324–37.
[16] Bower C, Rosen R, Jin L, Han J, Zhou O. Deformation of carbon nanotubes in nanotube-polymer composites. Appl Phys Lett 1999;74(22):3317–9.
[17] Yin M, Koutsky JA, Barr TL, Rodriguez NM, Baker RTK, Klebanov L. Characterization of carbon microfibers as a reinforcement for epoxy resins. Chem Mater 1993;5:1024–31.